Optoelectronic and thermoelectric properties of Zintl YLi_3A_2 (A = Sb, Bi) compounds through modified Becke–Johnson potential

T Seddik[1,†], G Uğur[2], R Khenata[1,‡], Ş Uğur[2], F Soyalp[3], G Murtaza[4], D P Rai[5], A Bouhemadou[6], and S Bin Omran[7]

[1] *Laboratoire de Physique Quantique et de Modélisation Mathématique, Université de Mascara, 29000 Algeria*
[2] *Department of Physics, Faculty of Science, Gazi University, 06500 Ankara, Turkey*
[3] *YüzüncüYıl University, Faculty of Education, Department of Physics, Van 65080, Turkey*
[4] *Materials Modeling Laboratory, Department of Physics, Islamia College University, Peshawar, Pakistan*
[5] *Department of Physics, Pachhunga University College, Aizawl, India-796001*
[6] *Laboratory for Developing New Materials and their Characterization, Department of Physics, Faculty of Science, University of Setif 1, 19000 Setif, Algeria*
[7] *Department of Physics and Astronomy, College of Science, King Saud University, P. O. Box 2455, Riyadh 11451, Saudi Arabia*

(Received 16 March 2016; revised manuscript received 12 June 2016; published online 25 August 2016)

In the present work, we investigate the structural, optoelectronic and thermoelectric properties of the YLi_3X_2 (X = Sb, Bi) compounds using the full potential augmented plane wave plus local orbital (FP-APW+lo) method. The exchange–correlation potential is treated with the generalized gradient approximation/local density approximation (GGA/LDA) and with the modified Becke–Johnson potential (TB-mBJ) in order to improve the electronic band structure calculations. In addition, the estimated ground state properties such as the lattice constants, external parameters, and bulk moduli agree well with the available experimental data. Our band structure calculations with GGA and LDA predict that both compounds have semimetallic behaviors. However, the band structure calculations with the GGA/TB-mBJ approximation indicate that the ground state of the YLi_3Sb_2 compound is semiconducting and has an estimated indirect band gap (Γ–L) of about 0.036 eV while the ground state of YLi_3Bi_2 compound is semimetallic. Conversely the LDA/TB-mBJ calculations indicate that both compounds exhibit semiconducting characters and have an indirect band gap (Γ–L) of about 0.15 eV and 0.081 eV for YLi_3Sb and YLi_3Bi_2 respectively. Additionally, the optical properties reveal strong responses of the herein materials in the energy range between the IR and extreme UV regions. Thermoelectric properties such as thermal conductivity, electrical conductivity, Seebeck coefficient, and thermo power factors are also calculated.

Keywords: Zintl compounds, TB-mBJ, electronic band-structure, optical properties, thermoelectric properties

PACS: 78.20.Ci, 79.10.−n **DOI:** 10.1088/1674-1056/25/10/107801

1. Introduction

In the past few years, Zintl compounds have been thoroughly investigated due to their characteristics which are desirable for an efficient thermoelectric material. These compounds are, in general, electronically positioned between intermetallic and insulating valence compounds. They are typically characterized by a small semiconductor band gap or semimetallic behavior and exhibit diverse and often complex crystal structures.

Among the Zintl phases, a ternary series adopting the $CaAl_2Si_2$-type structure has been vastly studied such as the AZn_2Sb_2 (A = Sr, Ca, Yb, Eu),[1–6] $XYZP_2$ (X = Ca and Yb; Y,Z = Zn, Mn, and Cu),[7] $CaZn_{2-x}Cu_xP_2$ and $CaMnZn_{1-x}Cu_xP_2$,[8] $EuMn_2Sb_2$,[9] $EuCu_2P_2$[10] compounds, etc. and this indicates their candidatures for thermoelectric applications. Many Zintl compounds of the $CaAl_2Si_2$ type are known, however its derivatives adopting the $LaLi_3Sb_2$-type structure, called the "filled" $CaAl_2Si_2$-type have attracted our attention due to their simple structures with diverse physical properties.[11–13] As ternary Zintl compounds, YLi_3X_2 (X = Sb, Bi) compounds possess the $LaLi_3Sb_2$-type structure. Using x-ray and neutron diffraction methods, these materials have been first investigated by Grund *et al.*,[11] and it was reported that these compounds crystallize into a "filled" $CaAl_2Si_2$-type structure each. To the best of our knowledge, there is scarce crystal structure experimental information of the YLi_3X_2 compound and in fact to date their optoelectronics and thermoelectric properties have not yet been calculated nor measured. For these reasons, the aim of the present work is to perform these calculations using the density functional theory (DFT).

2. Computational method

The calculations are performed using the full-relativistic version of the augmented plane wave plus local orbitals (APW+lo) method[14] in order to solve the DFT Kohn–Sham equation[15] as used in the WIEN2k computational code,[16] where the APW+lo and the linearized (L)APW+lo methods are some of the accurate methods of calculating the properties

†Corresponding author. E-mail: sedik_t@yahoo.fr
‡Corresponding author. E-mail: khenata_rabah@yahoo.fr

© 2016 Chinese Physical Society and IOP Publishing Ltd

of materials.[17,18] For structural properties, the generalized gradient approximation (WC-GGA) parameterized by Wu and Cohen[19] and the local density approximation (LDA)[20] are used for the exchange–correlation energy functional/potential. However, in order to calculate the optoelectronics and thermoelectric properties, the recently developed modification by Tran and Blaha (TB) of the Becke and Johnson (mBJ) exchange potential (TB-mBJ)[21] is used. This TB-mBJ functional describes the bandgaps of the insulators and semiconductors with high accuracy, which leads to an experimental agreement which is comparable to the calculations from hybrid functional or GW.[21] The values of muffin-tin sphere radius $R_{\rm MT}$ for the Y, Li, Sb, and Bi atoms are chosen to be 2.4, 2, 2.45, and 2.5 a.u. (atomic units), respectively. The calculations are performed with $R_{\rm MT}K_{\rm max} = 8.5$ (where $K_{\rm max}$ is the cut-off parameter for the plane wave) for the convergence parameter where the calculations are stable and convergent in terms of the energy. We use an appropriate set of k-points, consisting of the $12 \times 12 \times 6$ Monkhorst–Pack sampling, to compute the total energy. Furthermore, during the calculations of the electronic and optical properties, a dense k-grid of $17 \times 17 \times 9$ is utilized where the total energy convergence is guaranteed by varying both the plane wave cut-off parameter and the number of k-points.

3. Results and discussion

3.1. Structural properties

In ambient conditions, the YLi_3X_2 (X = Sb, Bi) compounds each crystallize into a $LaLi_3Sb_2$-type structure[11] in the space group P-3m1 (No. 164) as shown in Fig. 1. The conventional cell contains one formula unit with four independent Wyckoff sites: Li_1 on 1b, Li_2 on 2d (z_{Li_2}), Y on 1a, and X(= Sb, Bi) on 2d (z_X). Consequently, the crystalline structure of the YLi_3X_2 compound is characterized by three free parameters such as the lattice constant a, c/a ratio, and the internal structure parameters (z_{Li_2} and z_X). This is why we ought to relax the c/a ratio and z for each volume in order to obtain the optimized crystalline structure that minimizes the total energy and hence two sets of calculations are performed. The first one is that starting from the experimental lattice constants, we relax the internal parameters by relaxing the z coordinates of the second atom of the lithium and pnictide atoms until the forces on the ions are below a tolerance value taken at 0.001 eV/Å. The second one is that using the optimized internal parameters (z_{Li_2} and z_X), the total energy is calculated at different values of both volume V and c/a ratio, to achieve the minimum point in the total energy. Subsequently the calculated total energies versus volumes are fitted by the Murnaghan equation of state[22] in order to determine the ground-state properties such as the equilibrium parameters which are the equilibrium volume (V) of the unit cell, lattice constants a and c, bulk modulus B as well as its first pressure derivative B'. The deduced structural parameters obtained with both approximations are presented in Table 1, which are accompanied with some experimental data for comparison. Our estimated lattice constants a, c, and the c/a ratio, as well as the optimized internal parameters (z_{Li_2} and z_{Sb}), agree well with the available experimental data. The deviation between our calculated equilibrium lattice constants a, c via the GGA (LDA) approximation and the measured data are approximately 0.7% (0.37%), 1% (0.41%), and 0.04% (0.75%), 0.9% (0.27%) for the YLi_3Sb_2 and YLi_3Bi_2 compounds, respectively, which ensures the reliability of the presented first-principles computations in this paper. However for the bulk modulus no experimental data exists for these crystals so that a direct comparison of the calculated values of the bulk modulus is not possible.

Table 1. Calculated values of lattice parameters (a, c) (in unit Å), bulk modulus B (in unit GPa), pressure derivative of the bulk modulus (B'), and the internal parameters z_{Li_2}, z_X for the YLi_3X_2 (X = Sb, Bi) compounds as compared with the available experimental data.

System			a	c	c/a	z_{Li_2}	z_X	B	B'
YLi_3Sb_2	This work	GGA	4.499	7.083	1.574	0.647	0.247	48.10	4.16
		LDA	4.548	7.185	1.579	0.647	0.247	52.92	4.28
	Expt.[11]		4.531	7.155	1.58	0.647	0.247	–	–
YLi_3Bi_2	This work	GGA	4.603	7.223	1.569	0.649	0.244	42.76	4.11
		LDA	4.641	7.310	1.575	0.649	0.244	47.23	4.32
	Expt.[11]		4.606	7.29	1.58	–	–	–	–

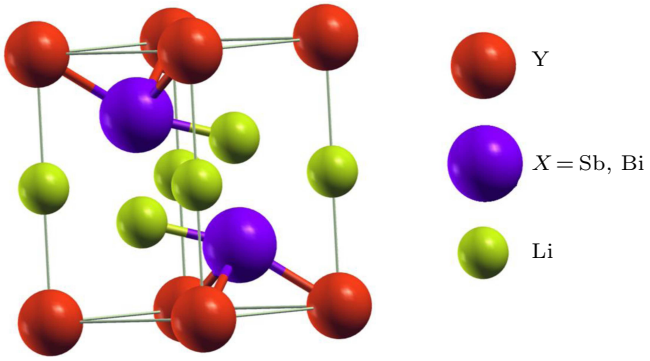


Fig. 1. (color online) Crystal structures of the YLi_3X_2 (X = Sb, Bi) compounds.

3.2. Electronic properties

In this subsection, we focus on the electronic properties of the YLi_3X_2 (X = Sb, Bi) compounds via calculating their energy band structures and the densities of states (DOSs). The calculated band structures at the equilibrium volumes of the YLi_3X_2 (X = Sb, Bi) compound within the WC-GGA and (GGA/ LDA) TB-mBJ approximation are shown in Fig. 2 for some high-symmetry directions in the Brillouin zone. This figure demonstrates that for the WC-GGA approach, the pnictides (Sb, Bi) p-like valence band and the yttrium d-like conduction band are found to cross over the Fermi level in the Γ

and L directions, respectively, so that there is a slight overlap among the conduction and valence bands. Hence, it indicates that the YLi_3X_2 (X = Sb, Bi) compounds are semimetal materials from the WC-GGA calculation which is the same as the result found from the LDA calculation. On the other hand, using the GGA/TB-mBJ approach this overlapping disappears, thus leading to a very small energy gap between the conduction and valence bands for the YLi_3Sb_2 compound, resulting in a semiconducting character with an indirect band gap (Γ–L) of about 36 meV [as shown in Fig. 2(a)]. However in the case of the YLi_3Bi_2 compound the lower edge of the conduction band (L-point) is equal to the highest edge (Γ-point) of the valence band in the energy band, which indicates a semimetal behavior [as shown in Fig. 2(b)]. Conversely the LDA/TB-mBJ calculation predicts a semiconducting character for both compounds with indirect band gap (Γ–L) values of about 0.15 eV and 0.081 eV for YLi_3Sb and YLi_3Bi_2, respectively. Moreover we include the spin–orbit coupling (SO) in our calculation for both approaches (GGA/LDA) TB-mBJ

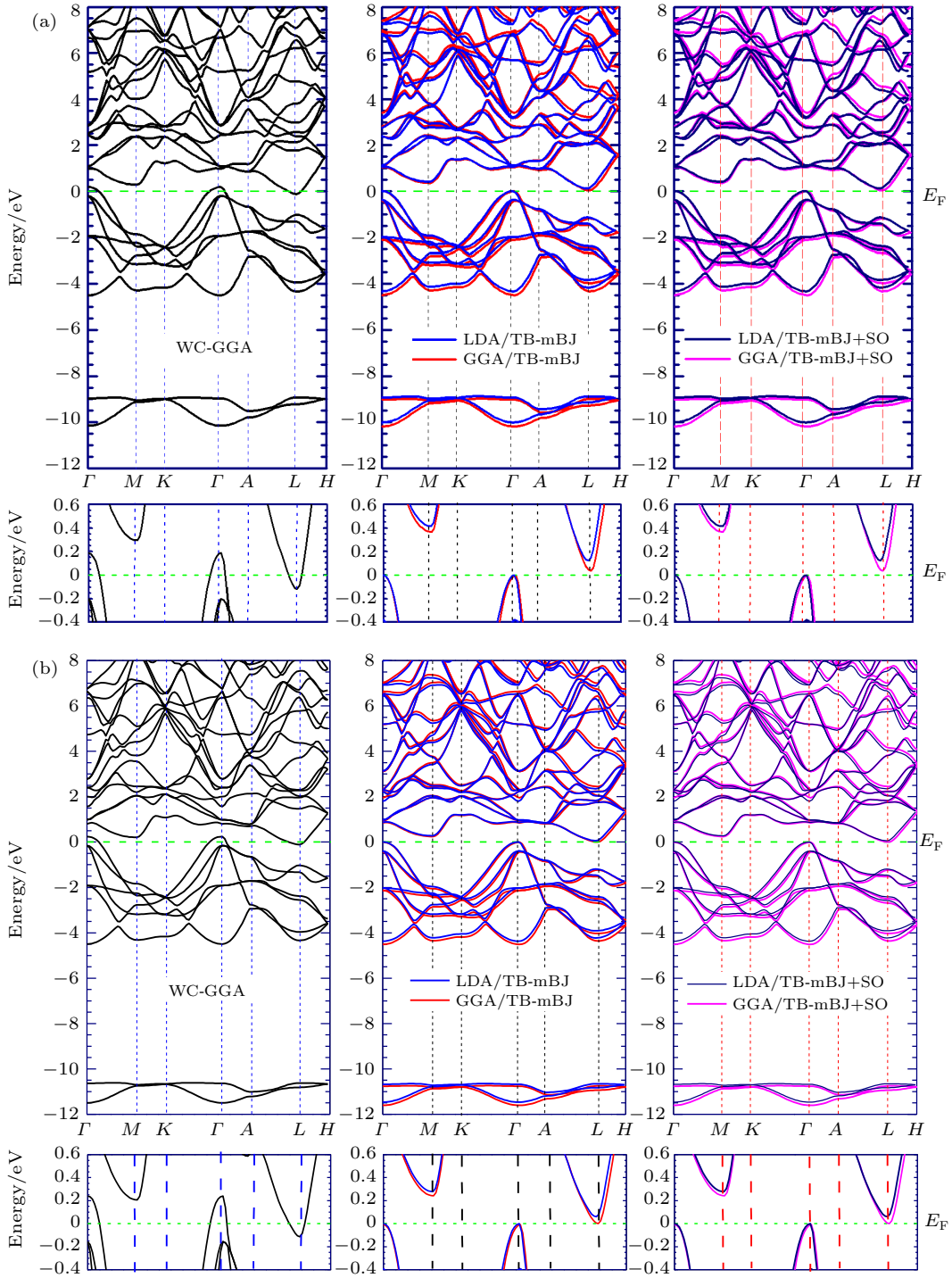


Fig. 2. (color online) Calculated band structures along some high symmetry lines in the Brillouin zone within the GGA, LDA/GGA-TB-mBJ with and without spin–orbit coupling approximations of (a) YLi_3Sb_2 and (b) YLi_3Bi_2 compounds.

as shown in Figs. 2(a) and 2(b). One can see that there are no great effects on the band structure calculations for both materials. The computed energy gap values are given in Table 2 and we mention here that no experimental nor theoretical work regarding the electronic properties is available for comparison. Nevertheless the overall band profiles of both the YLi_3Sb_2 and YLi_3Bi_2 compounds are found to have the same characteristic features as those of the $LaLi_3Sb_2$ compound.[12]

Table 2. Calculated values of direct and indirect band gap (in unit eV) within the LDA/GGA/TB-mBJ approximations with and without spin–orbit coupling (SO).

System		Γ–Γ	Γ–M	Γ–L
YLi_3Sb_2	GGA/TB-mBJ	1.01	0.38	0.036
	GGA/TB-mBJ + SO	1.02	0.38	0.037
	LDA/TB-mBJ	1.2	0.49	0.151
	LDA/TB-mBJ + SO	1.2	0.49	0.151
YLi_3Bi_2	GGA/TB-mBJ	0.85	0.23	0
	GGA/TB-mBJ + SO	0.86	0.23	0
	LDA/TB-mBJ	0.95	0.30	0.081
	LDA/TB-mBJ + SO	0.95	0.30	0.081

To attain a more in depth picture of the electronic structure, the total and partial atomic densities of states (TDOS and PDOS) for the YLi_3X_2 (X = Sb, Bi) compounds are calculated. Figure 3 shows the calculated TDOS and PDOS within the LDA/TB-mBJ approach. From this figure, the first thing that can be clearly seen is that the TDOSs of both compounds are each divided into three regions. The first region is a sharp peak represented by a flat band in the band structure (as shown in Fig. 2) between −11 eV and −9 eV as well as −12 eV and −10 eV in the valence band for the YLi_3Sb_2 and YLi_3Bi_2 compounds, respectively. This deep electronic localized structure arises mainly from the filled pnictides (Sb, Bi) "5s" states, which are separated from the upper valence band (UVB) by gaps of about 4.7 eV and 6 eV for the YLi_3Sb_2 and YLi_3Bi_2 compounds, respectively. The second region (UVB) lying between top of the valence band down to approximately −4.5 eV below the Fermi level (E_F) shows roughly two peaks with different intensities, in which the major contribution comes from the filled pnictide "5p" states mixed with the lithium "2s, 2p" states and the yttrium "4d" states. We note here the occurrences of an overlap between the X(= Sb, Bi) "5p", Y "4d", and the Li "2s, 2p" states in the valence states, which indicates a significant degree of hybridization between these states, thus suggesting covalent character on the X–Y and X–Li bond. The region above E_F is essentially dominated by the Y "4d" states mixed with the Li "2s, 2p" states, whereas the contributions from the pnictides (Sb, Bi) states are significantly reduced.

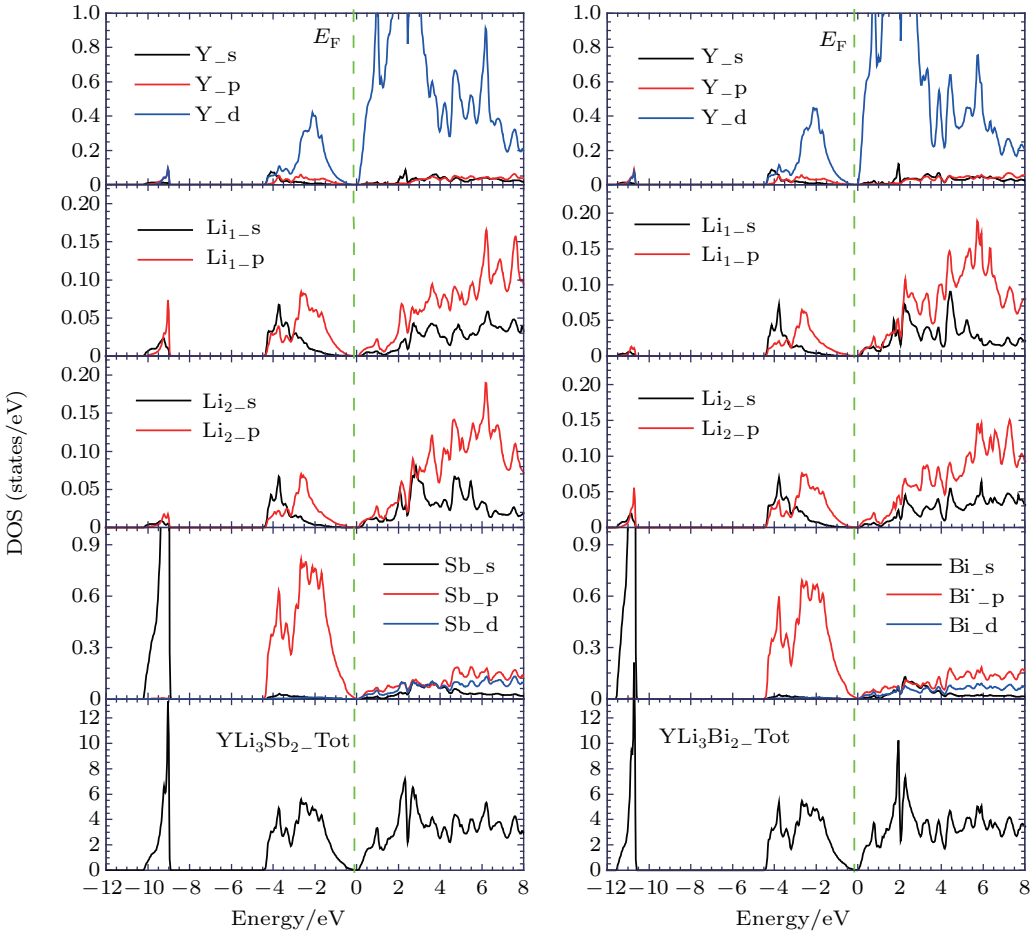


Fig. 3. (color online) Total and partial projected densities of states (TDOSs and PDOSs) for the YLi_3X_2 (X = Sb, Bi) compound within the LDA-TB-mBJ approximation.

3.3. Optical properties

We calculate the optical properties of the YLi_3X_2 (X = Sb, Bi) compounds based on the calculated LDA/TB-mBJ electronic structure for an incident photon of energy $\hbar\omega$ up to 40 eV. Figures 4(a) and 4(c) show the variations of spectrum of the imaginary part $\varepsilon_2(\omega)$ of the complex dielectric function with photon energy for the YLi_3X_2 (X = Sb, Bi) compounds, which corresponds to the photon-absorption caused by the electronic transitions from the occupied valence band (V_i) to the empty conduction band (C_i). We can see that for an energy range from 1 eV to 6 eV, the imaginary parts for each of both compounds present a considerable anisotropy between $\varepsilon_2^{\parallel}(\omega)$ and $\varepsilon_2^{\perp}(\omega)$. In this energy range, the $\varepsilon_2^{\perp}(\omega)$ spectra present three sharp peaks at about 2.08 eV, 2.91 eV, and 5.3 eV for the YLi_3Sb_2 compound and at about 1.87 eV, 2.83 eV, and 4.12 eV for the YLi_3Bi_2 compound. On the other hand, the $\varepsilon_2^{\parallel}(\omega)$ spectra of the YLi_3Sb_2 compound have three sharp peaks located at 1.56 eV, 3.78 eV, and 4.75 eV, respectively. However, for the YLi_3Bi_2 compound, there is one main sharp peak situated at 3.5 eV. These peaks are possibly generated mainly by the direct transition from the pnictides (Sb, Bi) "5p" states to the Y "4d" states and from the Li "2s, 2p" states to the Y "4d" states, respectively. Beyond this energy range, both the $\varepsilon_2^{\parallel}(\omega)$ and $\varepsilon_2^{\perp}(\omega)$ curves decrease rapidly with increasing photon energy and the anisotropy almost disappears. Moreover, at high energy, the imaginary parts of both compounds show small peaks at about 26.5 eV.

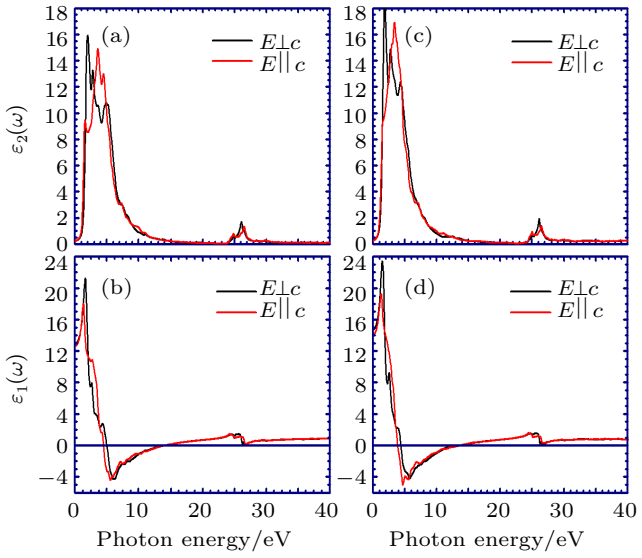


Fig. 4. (color online) Total and partial projected densities of states (TDOSs and PDOSs) for the YLi_3X_2 (X = Sb, Bi) compound within the LDA-TB-mBJ approximation.

The plots of the real part of the complex dielectric function, $\varepsilon_1(\omega)$ versus photon energy for the YLi_3X_2 (X = Sb, Bi) compounds as depicted in Figs. 4(b) and 4(d), each show dispersed electromagnetic energy when passing through a medium. An important quantity of $\varepsilon_1(\omega)$ is the zero frequency limit, $\varepsilon_1(0)$, which is defined as the low energy limit of the real part of the dielectric function and represents the dielectric response of a material to a static electric field. For both YLi_3Sb_2 and YLi_3Bi_2 compounds, the static dielectric constants, $\varepsilon_1^{\perp}(0)$ ($\varepsilon_1^{\parallel}(0)$) are found to be 12.94 (12.66) and 14.74 (14.08), respectively. Furthermore, the $\varepsilon_1^{\perp}(\omega)$, ($\varepsilon_1^{\parallel}(\omega)$) spectra show main peaks located at about 1.6 (1.33) eV for the YLi_3Sb_2 compound and at 1.54 (1.31) eV for the YLi_3Bi_2 compound in the visible light region. This is followed by a steep decrease until the $\varepsilon_1(\omega)$ spectrum becomes negative in the energy range where the phonon is damped, and then slowly increases towards zero. We point out that the real part $\varepsilon_1(\omega)$ of the dielectric function also presents anisotropy and consequently there are shifts of about 0.27 eV and 0.23 eV for the YLi_3Sb_2 and YLi_3Bi_2 compounds, respectively, between the main peak position of the $\varepsilon_1^{\perp}(\omega)$ and $\varepsilon_2^{\perp}(\omega)$ spectra.

From both the imaginary $\varepsilon_2(\omega)$ and the real $\varepsilon_1(\omega)$ part spectra of the complex dielectric function, the reflectivity coefficient $R(\omega)$, refractive index, $n(\omega)$ and the absorption coefficient, $\alpha(\omega)$ are calculated for the YLi_3X_2 (X = Sb, Bi) compounds against the photon energy, as shown in Fig. 5. At zero energy, the plots of reflectivity $R(\omega)$ versus photon energy of the YLi_3Sb_2 and YLi_3Bi_2 compounds as shown in Figs. 5(a) and 5(d) start at approximately 32% and 34%, respectively, and then increase with some oscillations in the energy range from 1 eV to 12 eV for the YLi_3Sb_2 compound and from 1 eV to 11 eV for the YLi_3Bi_2 compound, respectively. In addition, the $R^{\perp}(\omega)$ and $R^{\parallel}(\omega)$ spectra reach maximum values of 55% and 53% as well as 53% and 54% in the ultra-violet (UV) region for the YLi_3Sb_2 and YLi_3Bi_2 compounds, respectively, which coincides with the minimum values of the $\varepsilon_1(\omega)$ spectra. Subsequently, the reflectivity $R(\omega)$ shows a sharp drop at energies around 14.2 eV and 13.8 eV for both the YLi_3Sb_2 and YLi_3Bi_2 compounds, respectively, corresponding to the so-called screened plasma frequency (ω_P). Moreover, at an energy of about 26.5 eV, both the YLi_3Sb_2 and YLi_3Bi_2 compounds again exhibit reflectance values of approximately 12.8% and 12%, respectively, and then the magnitudes of the $R(\omega)$ spectra reach zero at high photon energy.

Figures 5(b) and 5(e) display the variations of refractive index $n(\omega)$ of the YLi_3X_2 (X = Sb, Bi) compounds with photon energy. Analyzing these dispersion curves we find that the static refractive indexes $n^{\perp}(0)$ and $n^{\parallel}(0)$ are about 3.59 and 3.55 and 3.83 and 3.75 for the YLi_3Sb_2 and YLi_3Bi_2 compounds, respectively. The $n^{\perp}(\omega)$ and $n^{\parallel}(\omega)$ spectra of both the YLi_3Sb_2 and YLi_3Bi_2 compounds increase from the static value to maximum values of 4.71 and 4.31, and 4.91

and (4.45), respectively, in the visible light region. Subsequently, the magnitude of the spectrum then decreases rapidly with photon energy to its minimum value which is smaller than 1 in the ultra-violet (UV) region.

Figures 5(c) and 5(f) show the plotted absorption coefficient spectra of the YLi_3X_2 (X = Sb, Bi) compounds. A wide absorption region is observed from the infrared (IR) to UV region with maximum values located at 6 eV and 5.6 eV for the YLi_3Sb_2 and YLi_3Bi_2 compounds, respectively. Furthermore at high energy, the materials exhibit strong absorptions in an energy range from 24 eV to 33 eV. Consequently, these results indicate that the YLi_3X_2 (X = Sb, Bi) compounds can absorb all of the frequencies between the IR and high UV regions.

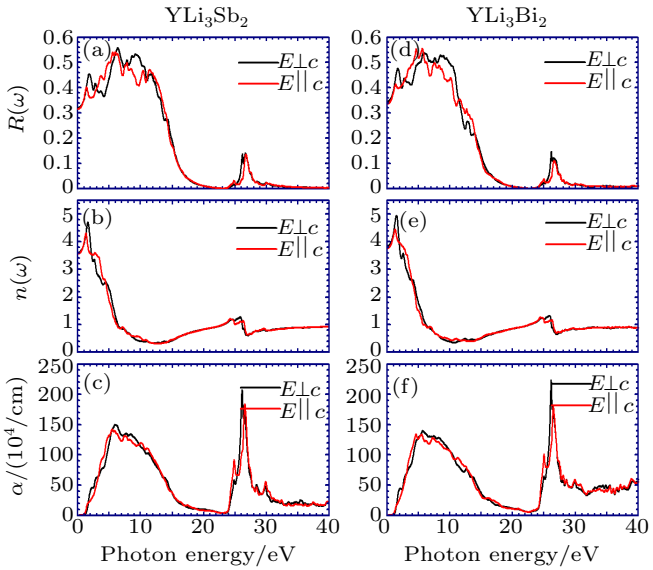


Fig. 5. (color online) Variations of calculated dielectric constants (reflectivity coefficient $R(\omega)$, refractive index $n(\omega)$, and the absorption coefficient $\alpha(\omega)$) with photon energy for YLi_3X_2 (X = Sb, Bi) compound.

4. Thermoelectric properties

The thermal energy can be converted into electrical energy by the thermoelectric materials. Therefore it is extremely interesting to study the thermoelectric properties of the YLi_3X_2 (X = Sb, Bi) compounds. The dependences of power factor, Seebeck coefficient, electrical conductivity, and thermal conductivity on temperature are important thermoelectric parameters.

In this work, the thermoelectric properties are predicted in a temperature range from 200 K to 800 K. Figure 6 shows the plots of electrical conductivity versus temperature and this parameter determines the free charge carrier flow. The electrical conductivity spectra of the examined compounds show that in the low temperature (200 K) region, the YLi_3Sb_2 and YLi_3Bi_2 compounds have electric conductivity values of $2.35 \times 10^{19}\,(\Omega \cdot \mathrm{m} \cdot \mathrm{s})^{-1}$ and $2.37 \times 10^{19}\,(\Omega \cdot \mathrm{m} \cdot \mathrm{s})^{-1}$ respectively. For the YLi_3Sb_2 compound, it initially decreases down to a temperature of 500 K and then it increases and reaches its maximum value at 800 K. On the other hand for the YLi_3Bi_2 compound, its electrical conductivity increases as the temperature increases and reaches its maximum value at a temperature of 800 K. Figure 6 shows that the YLi_3Sb_2 compound is a good electrical conductor compared with the YLi_3Bi_2 compound.

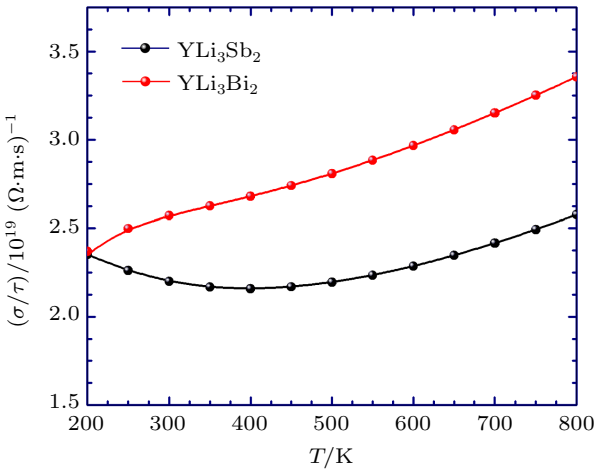


Fig. 6. (color online) Variations of calculated electrical conductivity per unit relaxation time with temperature for YLi_3X_2 (X = Sb, Bi) compound.

The variations of thermal conductivity with temperature of the compounds are shown in Fig. 7. At 200 K, the thermal conduction in the YLi_3Bi_2 compound is larger than that in the YLi_3Sb_2 compound where this trend is observed in the whole temperature range (from 200 K to 800 K). Maximum value of the thermal conductivity is noted to be 9.26×10^{14} W/m·K·s and 1.15×10^{15} W/m·K·s for the YLi_3Sb_2 and YLi_3Bi_2 compounds at 800 K, respectively. This shows that the YLi_3Bi_2 compound is a better thermal conductor at all temperatures than the YLi_3Sb_2 compound.

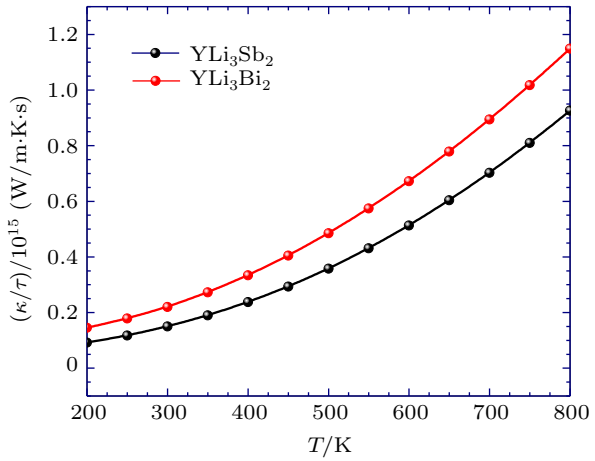


Fig. 7. (color online) Variations of calculated thermal conductivity per unit relaxation time with temperature for YLi_3X_2 (X = Sb, Bi) compound.

The Seebeck coefficient (S) is an important parameter that determines the efficiency of thermocouples and it is the ratio of the voltage difference to the temperature difference. The

variations of Seebeck coefficient with temperature of the compounds are shown in Fig. 8. The Seebeck coefficient has negative values for both compounds, showing that each of the compounds has an n-type conductivity. The maximum value of S is at 200 K and by increasing the temperature its value decreases for each of the compounds.

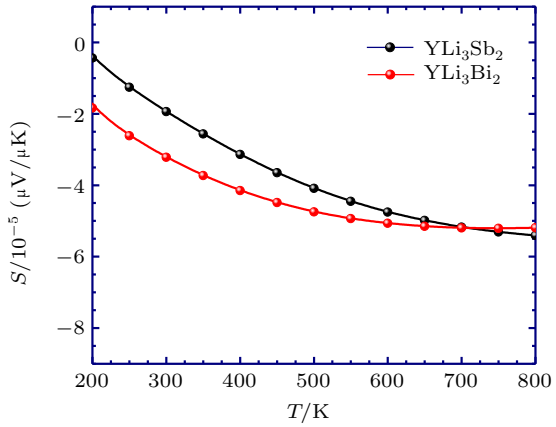


Fig. 8. (color online) Variations of calculated Seebeck coefficient with temperature YLi_3X_2 (X = Sb, Bi) compound.

Power factor is a parameter used to measure the electric power generation ability of a material. The calculated power factors per relaxation time of the YLi_3X_2 (X = Sb, Bi) compounds each as a function of temperature are shown in Fig. 9. At a temperature of 200 K, both compounds have low power factors, however the thermo power of the YLi_3Sb_2 compound is larger than that of the YLi_3Bi_2 compound. With temperature rising, the power factors are observed to gradually increase for both compounds. From the figure it is clear that the power factor reaches its maximum values of 9.04×10^{10} W/m·K^2·s and 7.53×10^{10} W/m·K^2·s (at 800 K) for the YLi_3Sb_2 and YLi_3Bi_2 compounds, respectively.

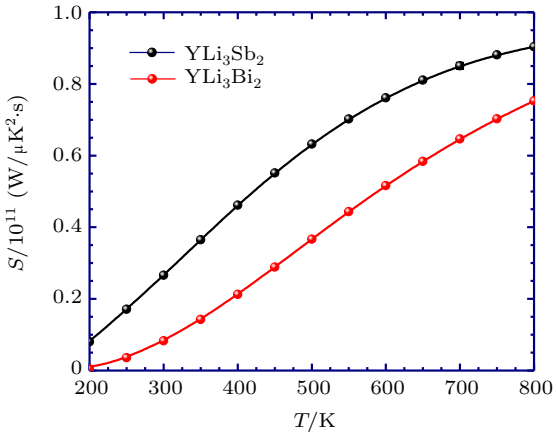


Fig. 9. (color online) Variations of calculated thermoelectric power factor temperature YLi_3X_2 (X = Sb, Bi) compound.

5. Conclusions

Using the APW+lo approach based on DFT, within the GGA/LDA and (GGA/LDA) TB-mBJ approximations, we perform a detailed investigation of the structural, optoelectronic and thermoelectric properties of the YLi_3X_2 (X = Sb, Bi) compounds with the $LaLi_3Sb_2$-type structure. Our estimated ground states' properties are in good agreement with the available experimental data. According to the electronic calculations, we find that both compounds exhibit semimetallic behaviors using the WC-GGA or LDA approach. However, employing the modified Becke–Johnson potential (GGA/TB-mBJ) semiconducting ground states are predicted for the YLi_3Sb_2 compound with an estimated indirect band gap (Γ–L) of about 0.036 eV and semimetallic ground states for the YLi_3Bi_2 compound. On the contrary the LDA/TB-mBJ calculations predict a semiconducting character for both compounds with indirect band gap (Γ–L) values of about 0.15 eV and 0.081 eV for YLi_3Sb and YLi_3Bi_2 respectively. Furthermore analyzing the DOSs of the herein materials we note a significant degree of hybridization between the X (Sb, Bi) "5p", Y "4d", and Li "2s, 2p" states in the valence states which suggest covalent characters on the X–Y and X–Li bonds. We also point out that the YLi_3X_2 (X = Sb, Bi) compounds each have a strong response in the energy range between the IR and extreme UV regions. The YLi_3Sb_2 compound is observed to be a better thermal and electrical conductor than the YLi_3Bi_2 compound, and the thermoelectric power of the YLi_3Bi_2 compound is larger than that of the YLi_3Sb_2 compound.

Acknowledgement

The authors (R Khenata, S Bin Omran and A Bouhemadou) extend their appreciation to the International Scientific Partnership Program ISPP at King Saud University for funding this research work through ISPP# 00.

References

[1] Toberer E S, Andrew F M, Brent C M, Espen F L and Snyder G J 2010 *Dalton Trans.* **39** 1046
[2] Zhang H, Zhao J T, Grin Y, Wang X J, Tang M B, Man Z Y, Chen H H and Yang X X 2008 *J. Chem. Phys.* **129** 164713
[3] Gascoin F, Ottensmann S, Stark D, Häile S M and Snyder G S 2005 *Adv. Funct. Mater.* **15** 1860
[4] Zwiener G, Neumann H and Schuster H U 1981 *Z. Naturforsch.* **36b** 1195
[5] Weber F, Cosceev A, Nateprov A, Pfleiderer C, Faißt A, Uhlarz M and Löhneysen H V 2005 *Physica B* **226** 359
[6] Weber F, Cosceev A, Drobnik S, Faißt A, Grube K, Nateprov A, Pfleiderer C, Uhlarz M and Löhneysen H V 2006 *Phys. Rev. B* **73** 014427
[7] Ponnambalam V, Lindsey S, Xie W, Thompson D, Drymiotis F and Terry M T 2011 *J. Phys. D: Appl. Phys.* **44** 155406
[8] Ponnambalam V and Donald T M 2014 *J. Electron. Mater.* **43** 1875
[9] Schellenberg I, Eul M, Hermes W and Pöttgen R 2010 *Z. Anorg. Allg. Chem.* **855** 636
[10] Artmann A, Mewis A, Roepke M and Michels G 1996 *Z. Anorg. Allg. Chem.* **622** 679
[11] Grund I, Schuster H U and Müller P 1984 *Z. Anorg. Allg. Chem.* **515** 151

[12] Schäfer M C, Suen N T, Raglione M and Bobev S 2014 *J. Solid State Chem.* **210** 89
[13] Winter F, Dupke S, Eckert H and Pöttgen R 2014 *Monatsh. Chem.* **145** 1381
[14] Madsen G K H, Blaha P, Schwarz K, Sjöstedt E and Nordström L 2001 *Phys. Rev. B* **64** 195134
[15] Hohenberg P and Kohn W 1964 *Phys. Rev. B* **136** 864
[16] Blaha P, Schwarz K, Madsen G K H, Kvasnicka D and Luitz J 2001 WIEN2k, "An Augmented Plane Wave Plus Local Orbitals Program for Calculating Crystal Properties", Vienna University of Technology, Austria
[17] Wong K M, Alay-e-Abbas S M, Shaukat A, Fang Y and Lei Y 2013 *J. Appl. Phys.* **113** 014304
[18] Wong K M, Alay-e-Abbas S M, Fang Y, Shaukat A and Lei Y 2013 *J. Appl. Phys.* **114** 034901
[19] Wu Z and Cohen R E 2006 *Phys. Rev. B* **73** 235116
[20] Perdew J P and Wang Y 1992 *Phys. Rev. B* **45** 13244
[21] Tran F and Blaha P 2009 *Phys. Rev. Lett.* **102** 226401
[22] Murnaghan F D 1944 *Proc. Natl. Acad. Sci. USA* **30** 5390
[23] Ambrosch-Draxl C and Sofo J O 2006 *Comput. Phys. Commun.* **175** 1
[24] Wooten F 1972 *Optical Properties of Solids* (New York: Academic Press)
[25] Sharma S, Verma A S, Bhandari R, Kumari S and Jindal V K 2014 *Mater. Sci. Semicond. Process.* **27** 79